In: Advanced Functional Polymers and Composites. Volume 2 ISBN: 978-1-62948-056-5
Editor: Inamuddin

Chapter 1

VOLTAMMETRIC NANOELECTRODE ENSEMBLES BASED ON TEMPLATED METAL NANOWIRES IN TRACK-ETCHED POLYMER MEMBRANES

***Michael Ongaro and Paolo Ugo*[1]**
Department of Molecular Sciences and Nanosystems,
University Ca' Foscari of Venice, Venice, Italy

ABSTRACT

This chapter reviews the recent advances taking place in the field of polymer based electrochemical sensors, in particular nanoelectrode ensembles (NEEs). In these sensors the polymer plays a crucial role in determining the specific characteristics and analytical performances. Synthetic approaches as well as principles of functioning and specific advantages and limits of NEEs are critically discussed. Useful examples of application to determinations of trace and ultratrace concentrations of inorganic and organic electroactive molecules of interest for environmental and biomedical analysis are given along with prospects in the future development of polymer based electrochemical sensors.

ABBREVIATIONS

3D-NEE	Three dimensional nanoelectrode ensemble
A_{act}	Active area
A_{geom}	Geometric area
AS-SWV	Anodic stripping square wave voltammetry
ASV	Anodic stripping voltammetry
CV	Cyclic voltammetry
D	Diffusion coefficient
DL	Detection limit
EDC	Carbodiimide

EL	Enzyme label
ELISA	Enzyme-linked immunosorbent assay
f	Fractional area
FA^+	(ferrocenylmethyl) trimethylammonium cation
Fc	Ferrocene
GOx	Glucose oxidase
HER2	Human epidermal growth factor receptor 2 protein
HRP	Horseradish peroxidise
I_C	Capacitive current
I_F	Faradic current
I_{lim}	Limiting current
I_p	Peak current
$k°$	Heterogeneous electron transfer rate constant
$k°_{app}$	Apparent heterogeneous electron transfer rate constant
MB	Methylene blue
MUC-16	Cancer marker Mucin-16
NEA	Nanoelectrode array
NEE	Nanoelectrode ensemble
PBE	Partially blocked surface electrode
PC	Polycarbonate
PET	Polyethylene terephthalate
q	Pore density
r	Pore radius
SAM	Self-assembled monolayer
SEM	Scanning electron microscope
ssDNA	Single stranded DNA
Sulfo-NHS	N-hydroxysulfosuccinimide
SWV	Square wave voltammetry
S/N	Signal-to-noise ratio
v	Scan rate
VB	Bulk etch rate
VT	Track etch rate
$W_{1/2}$	Half peakwidth
ΔE_p	Separation between the peak potentials
αMUC-16	Anti-Mucin-16 antibody

1. INTRODUCTION

Nanoelectrode ensembles (NEEs) are useful electroanalytical tools which are applied in many fields ranging from sensors to electronics as well as from energy storage/production to magnetic materials [1]. The first synthesis of NEEs prepared by using nanoporous membranes as templating material, was described by Menon and Martin [2] who deposited gold nanofibres with a diameter as small as 10 nm within the pores of track etched polycarbonate membranes by chemical (electroless) method. The result was a random ensemble of metal

wires surrounded by the insulating polymer; in this first example only the tips (approximately, in the shape of nanodisks) of the nanoelectrodes were exposed to the sample solution. All the metal nanowires were interconnected among each other by a metal back collector so that all the nanodisks experienced the same potential during electrochemical experiments. The scheme of the structure of a NEE is shown in Figure 1.

The template synthesis is based on the idea that the pores of a host material can be used as a template to direct the growth of new materials. Historically, the template synthesis in track-etched materials was introduced by Possin [3] and Williams and Giordano [4], who prepared different metallic wires with diameter as small as 10 nm within the pores of etched nuclear damaged tracks in mica. This method was indeed designed in order to image the shape of the pores rather than to obtain a functional composite with electrochemical sensing capabilities as prepared later by Martin [2]. Afterwards, various examples of membrane templated electrochemical deposition of nanowires of semiconductors [5], metals (e.g. Ni and Co) [6], oxides [7] and conducting polymers [1] appeared in the literature.

Also other approaches based on similar principles were tested to prepare NEEs, such as exploiting as nanoelectrodes the defects generated in self assembled monolayers [8,9,10], creating and controlling the pores in block copolymer self assembled matrices [11] as well as by exploiting chemical self-assembly of colloids [12]. Arrays of nanoelectrodes have been prepared also by using optical fiber bundles coated with gold [13,14] or by indium tin oxide [15] or by complex macroporous gold structures [16]. The chemical etching of the fiber bundle's distal end results in arrays of tips which are coated with the metal; individual nanotips can be obtained by coating the base of the fiber array with electrophoretic paint. Such devices present an interesting combination of optical and electrochemical properties.

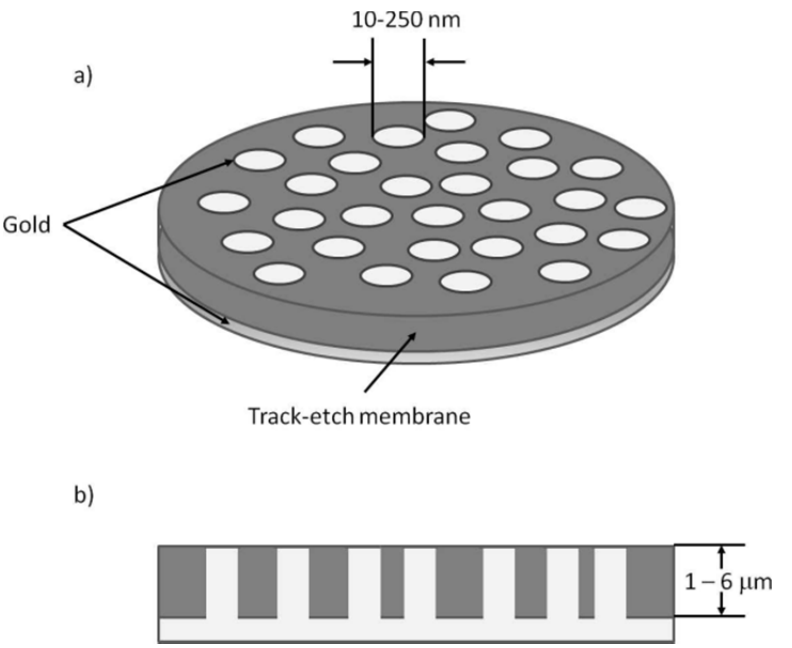

Figure 1. Scheme of a nanoelectrode ensemble in a template membrane(a) overall view; (b) lateral section.

In the template synthesis of nanoelectrode ensembles in track-etched polymers, each pore of the membrane is filled with a metal nanowire or nanofiber. The metal fibers growth can be performed both using electrochemical [6,17] or electroless deposition [2] methods. For the former case, one side of the membrane must be made conductive, for instance, by sputtering a thin layer of gold, while for the latter the chemical sensitization of the membrane is required [2,18,19].

With both deposition methods, the pore density in the template, determines the number of metal nanoelectrode elements on the NEE surface and, correspondingly, the average distance between them; while the diameter of the pores in the template determines the diameter of the individual nanoelectrodes. Track-etched membranes with pore diameters ranging from 10 nm to 10 μm are commercially available.

2. TRACK-ETCHED POLYMER MEMBRANES

The fabrication of nanoporous polymeric membranes by the track-etch method involves the exposure of a polymeric film to a beam of high energy particles to create damage tracks in the structure of the material (tracking). The tracks are subsequently etched to produce monodisperse pores by exposure to an alkaline solution (etching). It is possible to control the size and the density of the pores by changing the track-etch parameters. In fact, the longer the exposure of the polymer to the beam, the greater the number of tracks (and thus pores), while increasing the etching time (as well as the pH of the etching solution) it is possible to increase the diameter of the pores [20, 21].

Polymeric materials used for the production of track-etched membranes include poly(ethylene terephthalate) (PET), polycarbonate (PC), polyimide (Kapton), polypropylene, polyvinylidene fluoride, and CR-39 (allyl diglycol carbonate). PC is the material used for preparing the majority of commercially available track-etched membranes, because of its high sensitivity to tracking and low cost. PC is soluble in organic solvents and has low wettability in aqueous solutions; for this reason, in order to increase the hydrophilicity, the PC membranes are usually coated with polyvinylpyrrolidone [2].

On the contrary, PET membranes are relatively hydrophilic, rather stable to acids and organic solvents, and biologically inert, however, PET-tracked membranes require UV irradiation before etching, making them more expensive. The membrane is exposed to UV light with maximum intensity at 320 nm for approximately 30 min. The UV treatment leads to saturation of the damage in the tracks so that further storage of the samples in air or illumination with visible light does not change the etching behavior [22].

2.1. Tracking

There are two basic methods of producing latent tracks in the polymer foils to be transformed into porous membranes. The first method is based on the irradiation with fragments of the fission of heavy nuclei such as californium, bismuth, or uranium [23] of energy 11.4 MeV per nucleon [22,24]. To create an array of latent tracks penetrating the foil, a collimator is normally used.

The advantages of this tracking method are:

(a) good time stability of the particle flux;
(b) relatively low cost.

The limitations of the method are:

(a) contamination of the tracked foil with radioactive products ("cooling" of the irradiated material is needed, which usually takes few months);
(b) limited thickness of the membrane to be tracked;
(c) limited possibilities of controlling the angle distribution of the tracks;
(d) fragments of different masses and energies produce tracks with different etching properties [21].

The second method is based on the use of ion beams in accelerators [21]. The intensity of the ion beam should be at least 10^{11} sec^{-1}. To irradiate large areas, a scanning beam is normally used. The advantages of the ion beam accelerator tracking method are:

(a) no radioactive contamination of the material when the ion energy is below the Coulomb barrier;
(b) identity of the bombarding particles gives tracks with the same etching properties;
(c) large range of high-energy particles makes possible the tracking of thicker membranes;
(d) better conditions for producing high-density ($10^9/cm^2$) track arrays;
(d) particles heavier than fission fragments can be used (^{238}U, for example);
(e) it is easier to control the impact angle and produce arrays of parallel tracks or create some particular angular distributions [21].

Recent advances have shown that it is possible to control the number and the geometric distribution of tracks with an ion beam [24]. The sample is covered by a metallic mask with a hole of small diameter (0.1 mm) so that the ions can penetrate the film only within a small area. By registering the ions passing through the film and shutting down and moving the membrane after one single ion has passed through [24,25], it is possible to obtain single pore membranes or membranes with geometrically patterned arrays of tracks (and pores). The limitations of the ion beam accelerator method are:

(a) relative instability of the particle flux and
(b) higher cost than irradiation.

With the use of ion beams from accelerators, it is easier to control the impact angle for getting rid of merging pores of the kind shown in Figure 2 [21].

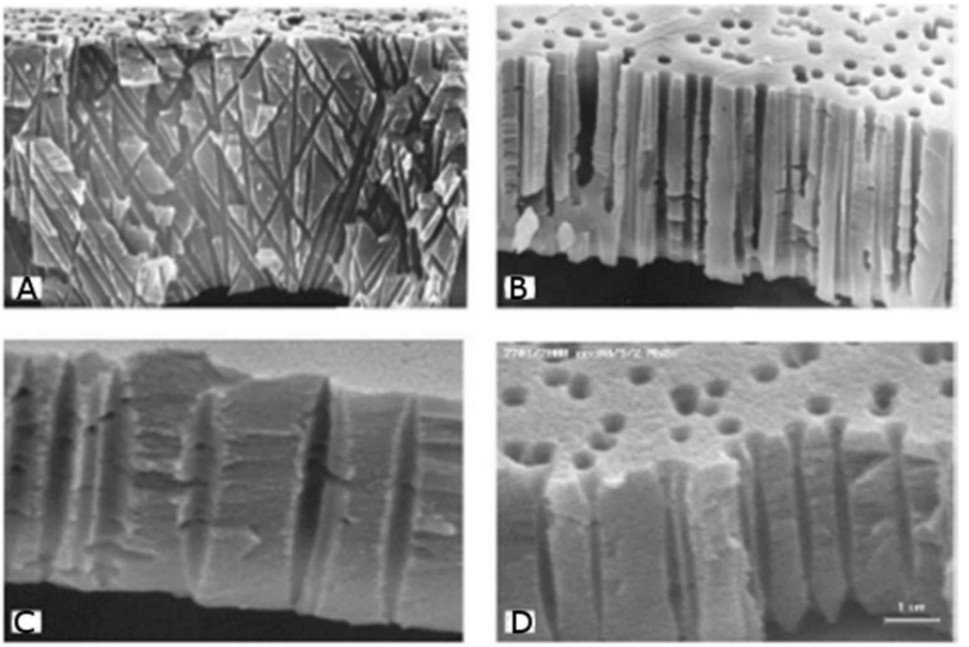

Figure 2. Porous structures obtained in polymeric films using different methods of irradiation and etching conditions: a) polycarbonate membrane with cylindrical, non-parallel pores; b) polypropylene with slightly conical parallel pores; c) polyethylene terephthalate with cigar shaped pores; d) polyethylene terephthalate with bow-tie pores [21]. Reprinted with permission from Apel, P. Y. *Radiat. Meas.* 2001, *34*, 559-566. Copyright © 2001, Elsevier.

2.2. Etching

Chemical etching is the process of pore formation during which the damaged zone of a latent track is removed and transformed into a hollow channel (pore) [21,23]. The most widely used etching agents are alkali solutions (KOH or NaOH), although the etching of polyimide (Kapton) requires an oxidizing agent such as NaClO [26]. The simplest description of the kinetics of the etching process is based on two parameters: the bulk etch rate (VB) and the track-etch rate (VT). While VB depends on the material, the etchant composition and the temperature, VT depends on additional parameters such as: the sensitivity of the material, irradiation, post-irradiation and etching conditions [21]. Etching with KOH or NaOH on both sides of the tracked membrane generates pores with a symmetric shape that are typically cylindrical or cigar-like (see Figure 2). The formation of cigar-like-shaped pores has been explained by two hypotheses [27]: (a) further exposure by electrons generated in the secondary electron cascade caused by the impact of the high-energy particle and (b) an acceleration of the etching rate caused by the etching products, which are more concentrated inside the pores. It was shown that perfectly cylindrical pores could be obtained if a special PC film (PC^+) is used instead of standard PC film [27].

It was recently shown that strict control of the etching conditions allows one to control the shape of the pores, obtaining, for example, funnel-like or conically shaped pores [22]. Conical pores can be obtained by asymmetric etching with oxygen plasma of initially cylindrical pores [28], or by performing an asymmetric chemical etching, so that VB > VT,

with the ratio changing throughout the thickness of the membrane. Asymmetric etching of tracked membranes was first described three decades ago [29]. It is based on the treatment of an ion-irradiated sample with an etchant on one side, while the opposite face is in contact with a stopping medium that neutralizes the etchant as soon as it perforates the sample. This method was modified recently by applying an additional electric field [24]. The scheme of the apparatus used for the asymmetric etching is shown in Figure 3. For asymmetric etching of PC or PET, one side of the membrane is put in contact with an alkaline etching solution, usually 9 M NaOH or KOH, and the other side is in contact with the stopping medium, typically a weak acid solution such as 1 M HCOOH in 1 M KCl [22]. For asymmetric etching of polyimide (Kapton), the etching solution is NaClO (with 13% active chlorine) while the stopping medium is a suitable reducing agent such as 1 M KI [30]. A potential of some tens of volts is applied across the membrane by two Pt electrodes. The electrode in the etching solution is positively polarized, while the electrode in the stopping solution is at a negative potential. The application of the electric field allows one to detect the instant of pore break-through and, additionally, to protect the etched cone pore from further chemical attack. If a positive potential is applied from the alkali (etchant) side during the break-through, the OH^- anions are pulled out of the pore which accelerate the stopping process. It was demonstrated [22] that electrostopping at voltages around 1 V is more efficient in producing conical pores than chemical stopping alone. The application of a potential across the membrane is stopped as soon as a monitoring ammeter records an increase in the current that passes through the membrane up to reaching a pre-set value, typically 1 mA. The membrane is then immediately immersed (both sides) in the stopping medium, thus blocking the asymmetric etching. At the end of the process, conical nanopores of controlled shape are obtained [28,31]. It was also shown that the addition of alcohols (such as methanol, ethanol, or propanol) to the etch solution allows further control of the etching rate and the V_B/V_T ratio [31,32]. Several analytical and bioanalytical applications of conical nanopores have been recently presented [33,34,35].

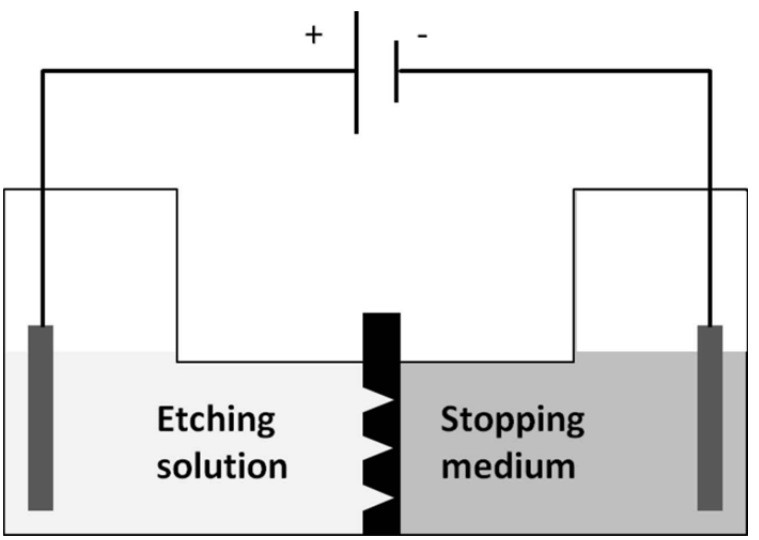

Figure 3. Scheme for the experimental set-up with the etching cell for asymmetric pore etching.

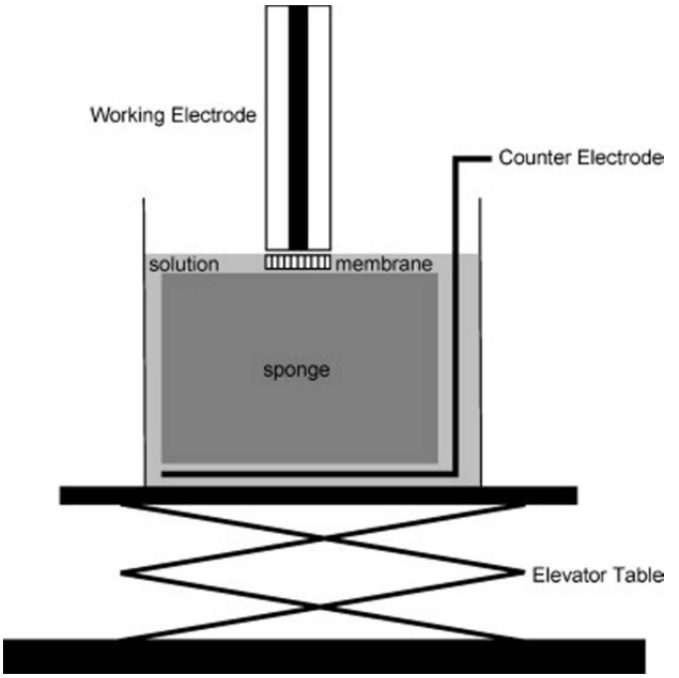

Figure 4. Scheme of the cell setup used in ref. [36] for electrochemical template deposition. Rising the elevator the membrane lying over the sponge, soaked with the electrolyte, is pressed on the surface of the electrode [36]. Reprinted with permission from Gambirasi, A. et al. *Electrochim. Acta* 2011, *56*, 8582-8588. Copyright © 2011, Elsevier.

3. TEMPLATE DEPOSITION OF METALS

3.1. Electrochemical Deposition

The electrochemical deposition inside the pores of a porous membrane requires that one side of the membrane be made conductive. This can be done by plasma or vacuum deposition of a thin layer of metal (typically, 100 - 200 nm) on one side of the membrane. The metal layer can be the same or different from the metal which will be electrodeposited inside the pores and the membrane should be robust enough to tolerate this kind of treatment. As an alternative, it is possible to place the membrane directly in contact with a solid electrode. Figure 4 shows the interesting cell setup recently proposed by Gambirasi et al. [36], in which the membrane is placed between a solid electrode and a sponge drenched in the electrolyte, the pressure made by the electrode on the sponge keeps the membrane tightly fixed to the electrode for the time of the deposition. In electrochemical template deposition, the coated film is placed in an electrochemical cell, acting as the cathode and a counter electrode is the anode.

The deposition can be conducted in potentiostatic or in galvanostatic conditions. In the former case, it is possible to monitor the time course of the deposition and the progressive filling of the pores by analyzing the time transient current. As shown in Figure 5, the deposition curve can be divided in four parts [37,38] (denoted I-IV, Figure 5) associated to the four steps of the deposition sketched in Figure 6. Immediately after closing the circuit

(phase I) the current shows an intense peak and a fast decay due to the depletion of metal ions following the fast initial deposition and the increase of resistance inside the pores of the membrane. Subsequently, the current slowly decreases (phase II) while the deposition proceeds and the pores are filled. During phase III, the current increases again due to the increase of the electrode area subsequent to the emersion of the metal from the pores. In this phase it is possible to observe caps on the tips of the nanowires with a typical mushroom shape [6]. Finally the overgrown caps merge together into an almost flat surface leading to a plateau in the current transient (phase IV). For the sake of NEE preparation it is essential to stop the electrodeposition at the end of stage two, before the "mushroom caps" start to grow.

Since the process is based on the progressive growth and filling of the pores from the bottom metallic layer toward the open end of the pores, final products are nanowires and not hollow structures (e.g. nanotubes).

Electrodeposition of metals has been studied to obtain gold nanowires, but also other materials, such as, for instance, metals (Co [5,39,40] Ni [5,37,41] Cu [5,37], Pt and Pd [42]), alloys (NiFe [40], FeSiB [41]) or salts (Bi_2Te_3 [43], CdS [44]) have been investigated.

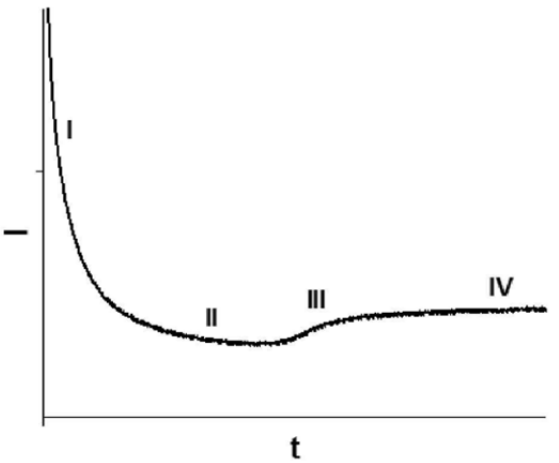

Figure 5. Time transient current for the electrochemical deposition using a track-etch membrane as templating material.

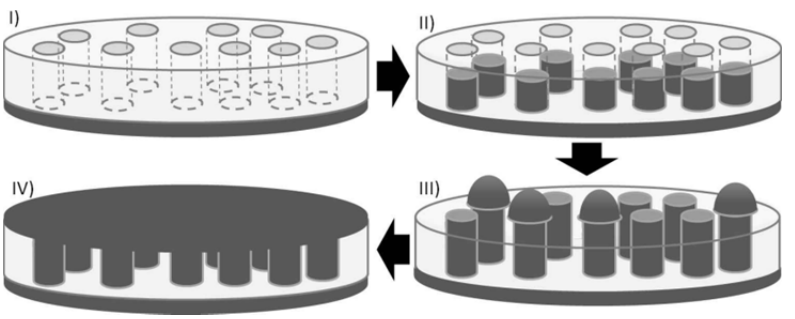

Figure 6. Schematic illustration of the stages of metal nanowires formation by electrochemical template deposition. I) Nucleation of metal crystallites at the pore base; II) pore filling with metal; III) emersion of the metal from the pores and caps formation; IV) caps merge together into a flat surface.

One problem encountered during the electrodeposition of metals inside polycarbonate membranes is related to the low wettability of this polymer even after impregnation with polyvinyl pyrrolidone. To overcome this problem, Mallouk et al. [45,46,47,48] proposed the addition of a small amount (1-2 %) of gelatin inside the electrodeposition bath.

3.2. Electroless Deposition

The electroless deposition involves the chemical reduction of a metal salt from the solution to a surface. Noncatalytic surfaces, such as nonconductors, have to be activated (made catalytic) prior to the electroless deposition. Usually, this is performed by generating metal nuclei on the surface of the noncatalytic material. In this way, the metal ion is preferentially reduced at the sensitized surface so that only this surface is plated with the desired metal [49].

The principles of electroless deposition on nanoporous membranes are exemplified by the Au deposition method developed in Charles Martin's laboratory [1,2] for the template fabrication of NEEs, nanotubes and other shaped gold materials. The electroless deposition of gold can be divided in four steps: a)"sensitization" of the membrane, adsorbing Sn^{2+} ions on the substrate; b) the Sn^{2+} ions act as reducing agent on the surface of the membrane for the formation of Ag nanoparticles; c) galvanic displacement of Ag particles by reduction of gold ; d) catalytic reduction of more gold by addition of a reducing agent (formaldehyde).

A detailed description of the gold electroless deposition process is the following [2,50,51]. After wetting for 2 h in methanol, the PC membrane is sensitized by immersion into a 0,026 M $SnCl_2$ solution and 0,07 M CF_3COOH in 50:50 methanol/water for 45 minutes. The membrane is, successively, immersed in a 0,029 M $Ag[(NH_3)_2]NO_3$ solution for 10 minutes. The solution is prepared by dropwise addition of concentrated NH_4OH to a 0.029 M $AgNO_3$ aqueous solution. At the first NH_4OH addition, a brown precipitate should appear and then disappear with further addition of NH_4OH, as soon as the precipitate disappears the solution is ready for use. Afterward the membrane is immersed into a gold plating bath ($7.9 \cdot 10^{-3}$ M $Na_3[Au(SO_3)_2]$ and 0.127 M Na_2SO_3) which is kept at 0°C. After 20 minutes, 1 mL of formaldehyde (37 %) is added and after 1 hour an additional mL of formaldehyde (37 %) is added. The deposition is then allowed to proceed for another 23 hours after which the membrane is rinsed with deionized water and immersed in HNO_3 (10 %) for 12 hours. The membrane is finally rinsed again with water and dried, resulting in the deposition of continuous gold nanowires within the pores and on both sides of the membrane faces.

In contrast to the electrochemical template deposition, in the electroless method the metal layer grows from the catalytic nuclei (which are located on the pore walls) towards the center of the pores. For this reason it is possible to stop the deposition at short times in order to obtain hollow tubes instead of nanowires. This procedure allows to obtain microfiltration membranes with golden pores [52,53] which can be further functionalized, for example with thiols [54], showing interesting applications as molecular sieves. A sensitive detection approach based on such modified membranes involves the application of a constant potential across the membrane and measuring the drop in the trans-membrane current upon the addition of the analyte. Detection limits as low as 10^{-11} M were obtained [55].

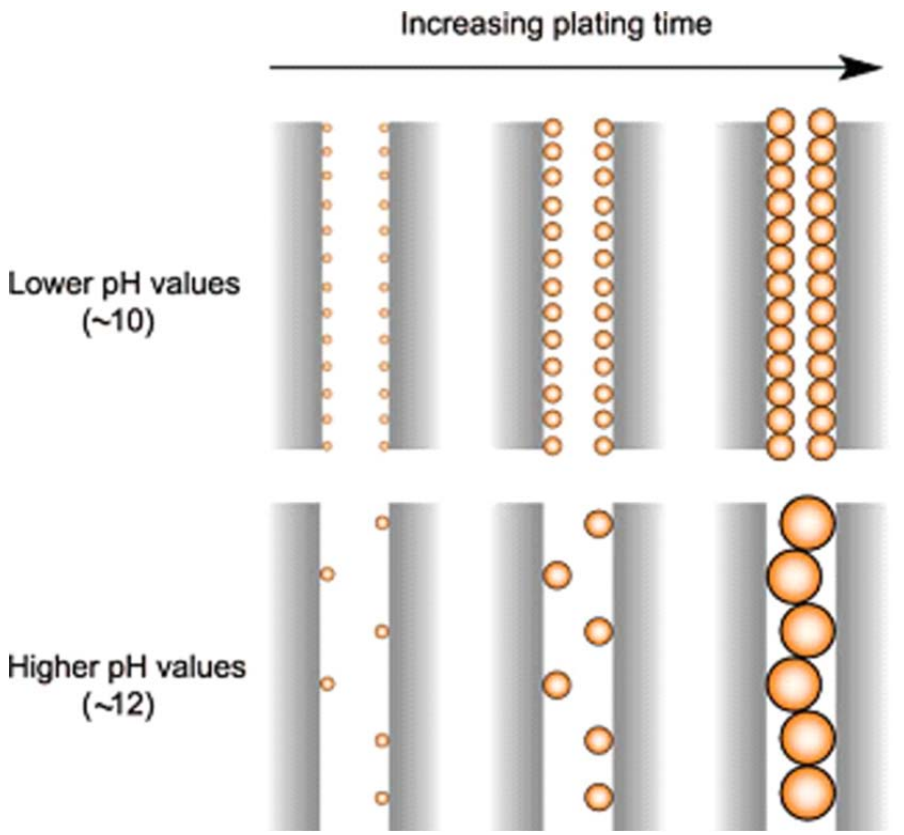

Figure 7. Schematic illustration of the particle growth within pores with a diameter of approximately 30 nm comparison of the situation at pH 10 and pH 12 after a few minutes (on the left), 0.5–1 h (in the middle), and 2–5 h (on the right) [18]. Reprinted with permission from De Leo, M. et al. *Chem. Mat.* 2007, *19,* 5955-5964. Copyright © 2007, American Chemical Society.

Also other metals, such as Cu [56], Pd [57] and Ni-P [58] can be deposited in polycarbonate templates by electroless deposition. In this case a suitable procedure for the desired metal has to be applied.

When the goal of the deposition is to obtain freestanding metallic structures then it is possible to completely etch the template. Polycarbonate can be dissolved by organic solvents, such as CH_2Cl_2/C_2H_5OH mixtures [59,60], or, as an alternative, by etching with plasma oxygen [61].

The results of an in-depth analysis of the experimental parameters, such as solution pH, activation and deposition time, on the final result of the template electroless depositions, have been recently reported [18,19]. The pioneering observations by Martin's group [2] demonstrated that the electroless deposition process always starts with the formation of gold nuclei on the pore walls and the growth of these nuclei is strongly pH dependent. At high pH, the process is faster and continuous nanowires are obtained (Figure 7). However, at lower pH, the growth of the nuclei is slower and gold nanotubes, (composed by the slow coalescence, on the pore walls, of the starting gold nuclei) can be obtained (Figure 7).

For the preparation of NEEs, continuous gold nanowires are preferentially grown and kept inside the pores of the membrane, obtaining a polycarbonate/ gold nanowires composite.

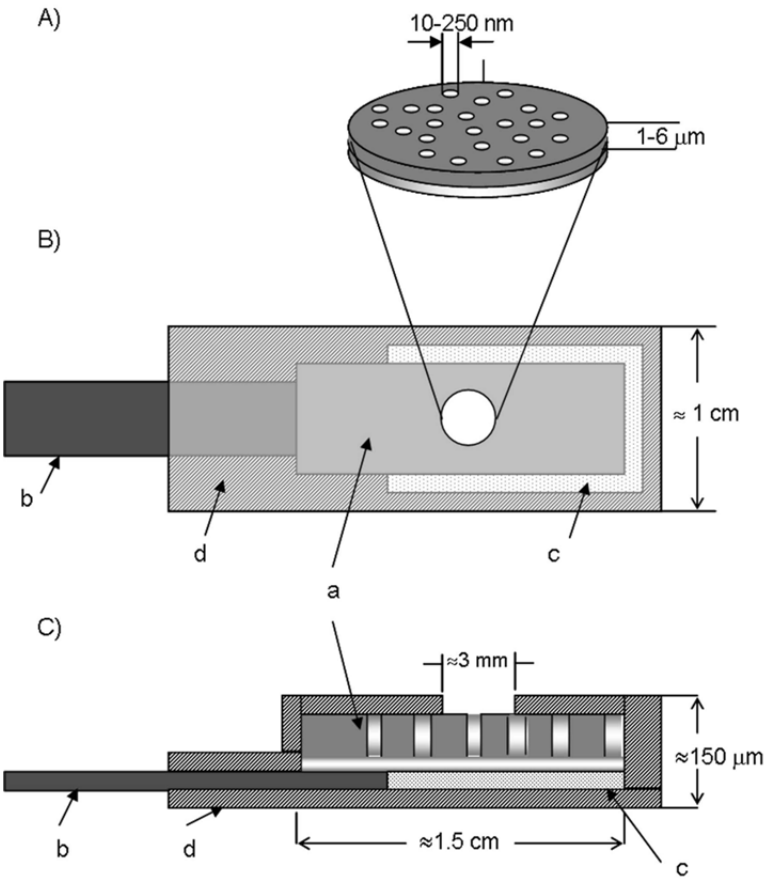

Figure 8. Scheme of a NEE prepared using a track-etched polycarbonate membrane as template A). Particular of the section of the active area; B) top view, C) section of the all NEE ready for use as working electrode. (a): track-etched golden membrane; (b): copper adhesive tape with conductive glue to connect to instrumentation; (c): aluminum adhesive foil with non-conductive glue; (d): insulating tape. Note: the dimensions of the pores (nanofibers) are only indicative and not in scale [64]. Reprinted with permission from Ugo, P.; Moretto, L. M. In *Handbook of Electrochemistry*; Editor, C. Zoski, Elsevier: Amsterdam, 2007; pp 678-709. Copyright © 2007, Elsevier.

4. NEES FABRICATION (FROM A GOLDEN MEMBRANE TO AN ADVANCED ELECTRODE)

Specific details on how to assembly handable NEEs, to be used for practical electrochemical and analytical purposes, can be found in the first original papers as well as in more recent reviews [2,18, 59,62,63,64]. The starting material for the NEE preparation is a piece of a golden polycarbonate membrane, with both faces covered and the pores filled with gold. The smooth side of the membrane is peeled off with adhesive tape (3M scotch Magic^{TM}) so that the tips of the nanowires remain exposed on one side. The exposed tips will become the active surface of the electrode. A piece of copper adhesive tape (5x60 mm) with conductive glue (Ted Pella, Inc.) is first affixed on a small adhesive non conductive aluminium square and then to the lower Au coated surface of a 5x5 mm piece of peeled

membrane, so that only a small part is in contact with the copper tape. This is because the conductive glue on the copper tape contains Ni particles which could damage the membrane [2]. Finally, strips of non conductive tape are applied to the lower and upper sides of the assembly in order to insulate the aluminium and copper tape. This can be done using a piece of adhesive insulating tape or plastic shrinkable adhesive films, such as Topflite Monokote or similar. A circular hole with an area typically of 0.07 cm^2 is punched into the upper piece of insulator prior to its placement on the assembly. This hole defines the geometric area (A_{geom}) that is the area exposed to the solution and defines the geometric area of the NEE. Note that A_{geom} can indeed be changed at pleasure, e.g. from 0.03 to 3 cm^2 [65], without influencing the high signal/noise (S/N) ratio typical of NEEs (see paragraph 6.2). As a final step, the NEE assembly is heat-treated at 150°C for 15 minutes. This procedure produces a water-tight seal between the gold nanowires and the surrounding polycarbonate. A scheme of a NEE is reported in Figure 8.

5. Ordered Arrays of Nanoelectrodes by Nanolythography

A recent advance on the use of PC for preparing arrays of nanoelectrodes (NEA), come from the demonstration that polycarbonate can be successfully used as high resolution resist for e-beam lithography. The method is based on the implementation of e-beam lithography, for the high resolution tracking of the polycarbonate[66].

The proposed process, summarized in Figure 9, is based on the spin-coating of a thin PC layer on silicon wafer coated by Si_3N_4, a Cr or Ti interlayer (to improve adhesion) and finally an Au layer. The PC surface is exposed to the e-beam and the tracks developed (etched) in KOH.

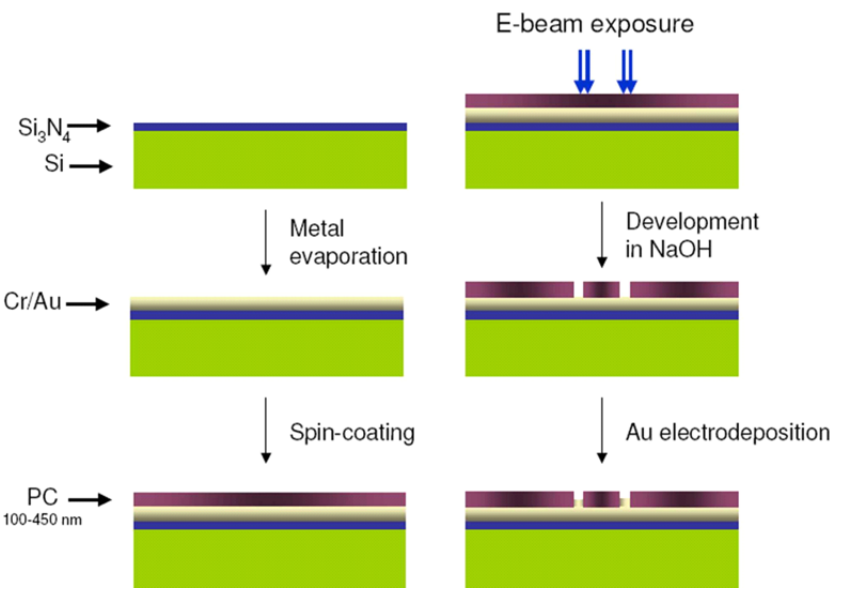

Figure 9. Scheme of preparation of a NEA by using e-beam lithography on PC.

As shown in Figure 10, thanks to the good properties of PC, as a high resolution e-beam resist, by this way it is possible to obtain perfectly ordered array of nano-holes with controlled diameter.

These holes can already be used as gold recessed nanoelectrodes, however by further electrochemical deposition of gold, it is possible to fill partially or totally the holes up to obtain arrays of inlaid nanodisk electrodes (Figure 11).

The perfect control of the geometry of the array allows the full control of the diffusion regime at the NEA (see paragraph 6.1). Note that similar procedures have also been developed using polymers different from PC, as well as different nanolithographic tools [67,68,69].

The advantages of using PC include its good quality and easy use as high resolution e-beam resist as well as the possibility to functionalize it with biomolecular recognition layers, using already known functionalization methods [70,71].

6. Electrochemistry with Polymer Templated Nanoelectrodes Ensembles and Arrays

6.1. Diffusion at Arrays/Ensembles of Nanoelectrodes

From a voltammetric viewpoint, a NEE/NEA can be considered as an assembly of ultramicroelectrodes separated by a non-conductive substrate. An ultramicroelectrode is an electrode with at least one dimension lower or comparable to the thickness of the diffusion layer (< 25 μm). At such range scale, the edge effects become relevant and the diffusion from the bulk of the solution can be described with a radial geometry instead of a linear one which is typical for larger electrodes (>100 μm). In radial diffusion regime, the voltammograms are defined by a sigmoidal shape, where the limiting current (I_{lim}), and not the peak current, is the key parameter directly related to the analyte concentration.

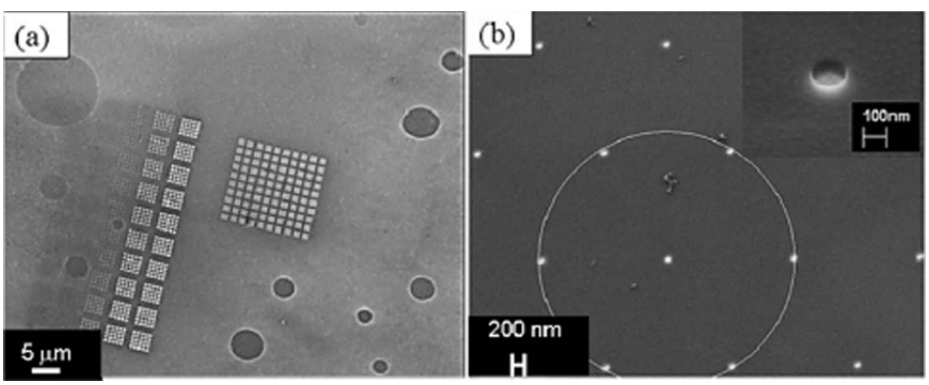

Figure 10. a) SEM micrograph of a nanohole matrix on PC membrane, obtained by e-beam lithography, development at 70°C for 60 s and subsequent electrochemical gold deposition. b) Top view of 75 nm radius dots in a hexagonal array on PC film; inset: higher magnification detail [66]. Reprinted with permission from Moretto, L. M. et al. *Nanotechnology* 2011, *22*, 185305-185312. Copyright © 2011, IOP Publishing.

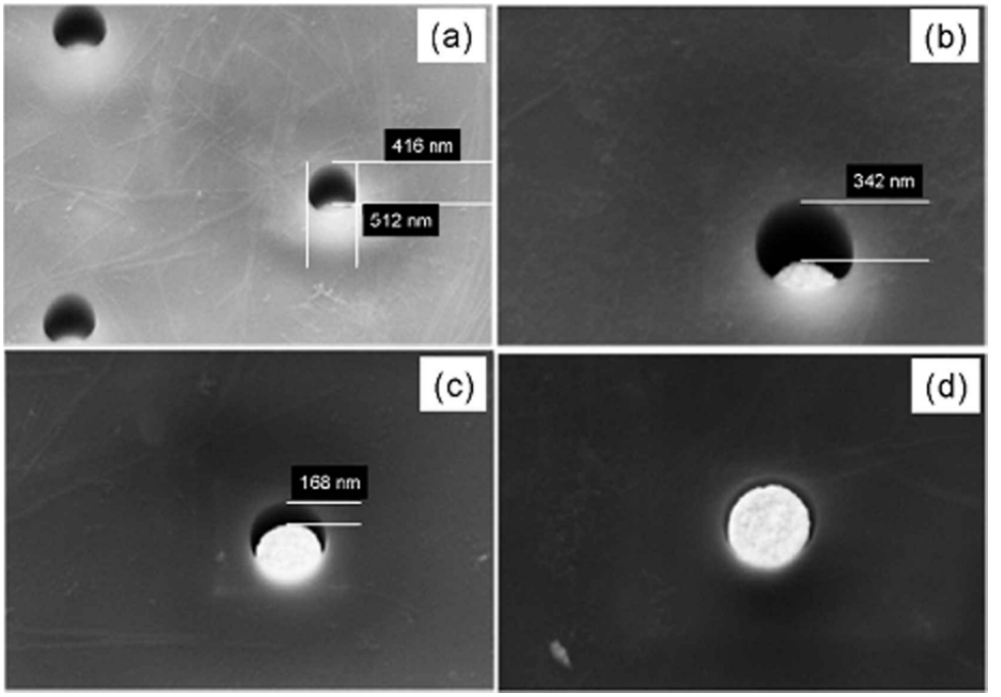

Figure 11. SEM images of NEAs with holes of 500 nm in diameter with gold electrochemically deposited inside for 0 s (a), 10 s (b), 20 s (c) and 30 s (d). Estimated recession depths: (a) 450 nm; (b) 300 nm; (c) 150 nm; (d) 0 nm [66]. Reprinted with permission from Moretto, L. M. et al. *Nanotechnology* 2011, *22*, 185305-185312. Copyright © 2011, IOP Publishing.

In an array, every gold disk can be considered as an ultramicroelectrode whose dimension and density are defined respectively by the pore diameter and by pore density of the templating membrane.

A typical density (q) of nanodisks/surface in a NEE, obtained from track-etched membranes, is as large as 10^6-10^8 elements/cm^2, that is large enough to make all the nanoelectrodes statistically equivalent so that the different contribution of the elements at the outer range of the ensemble can be considered negligible, [65,72] even in NEEs of overall area as small as 10^{-2}-10^{-3} cm^2 [65].

NEEs can exhibit different voltammetric responses depending on the scan rate or the reciprocal distance among the nanoelectrodes [73,74]. Different situations are summarized in Figure 12. When radial diffusion boundary layers totally overlap, i.e. when the diffusion hemisphere is larger than the mean hemidistance among the nanoelectrodes, NEEs behave as macroelectrodes with respect to the Faradic current (total overlap regime, peak shape voltammograms, case V). When the diffusion hemisphere becomes shorter (higher scan rates) or the hemidistance among nanodisks is larger, the voltammetric response is dominated by radial diffusion conditions at each element (pure radial regime, sigmoidally shaped voltammograms, case III). At very high scan rates, the linear active state is reached, where linear diffusion is predominant at each nanodisk (peak shaped voltammograms, but with peak currents much smaller than case V, case I). In cases II and IV intermediate situations can be observed.

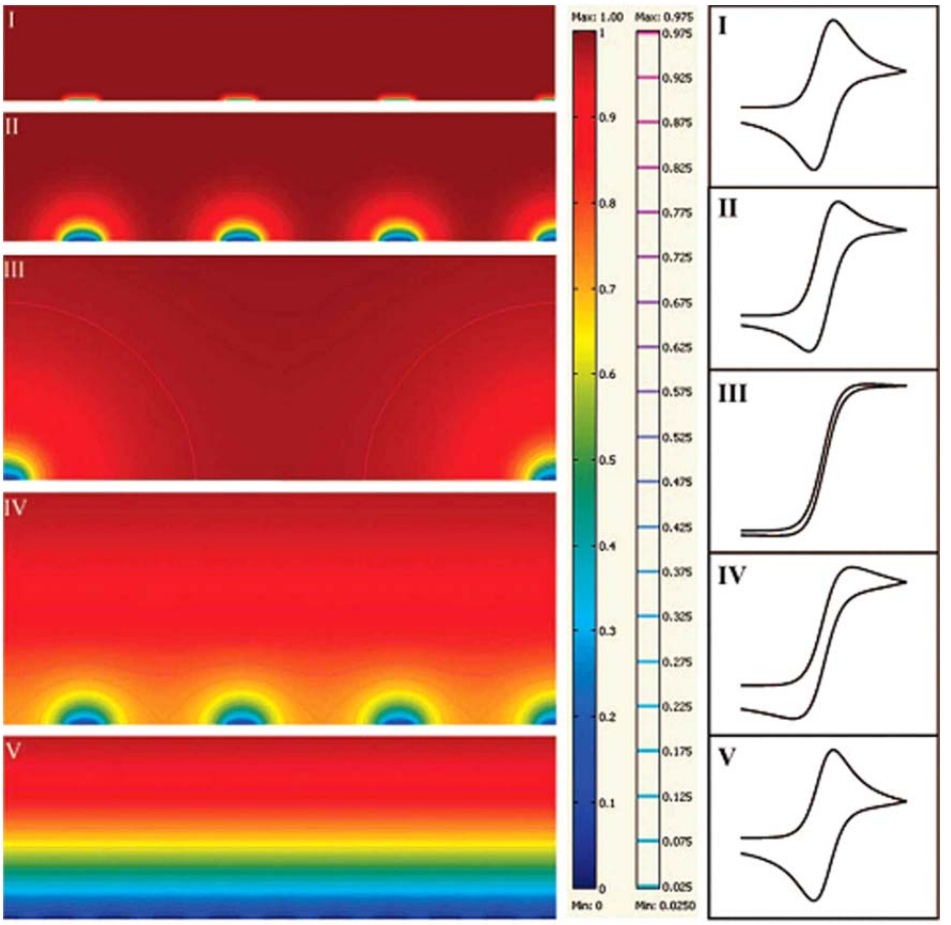

Figure 12. Simulated concentration profiles with isoconcentration contour lines, over a microelectrode array representing the five main categories of diffusion modes (form I to V). In the scale bar next to the figure, the red color represents the bulk concentration and the blue color represents zero concentration. The second scale bar represents a relative concentration scale for the contour lines. Typical CVs of the each category are shown at the right [75]. Reprinted with permission from Guo, J. et al. *Anal. Chem.* 2009, *81*, 130-138. Copyright © 2009, American Chemical Society.

Recent theoretical studies [72,75,76,77,78] examined in detail the role of the different diffusion regimes on the voltammetric responses recorded at NEE/NEAs. Guo and Lindner [75] introduced a very useful zone-diagram where the combination of suitable adimensional parameters allows one to determine the diffusion regime (as kind of voltammetric response) operative at a certain kind of array, at a specific voltammetric scan rate (see Figure 13).

Note that such a simulation was developed for arrays in which the effect at the border of the array is negligible; that is for array including a very large number of nanoelectrodes. This is indeed the situation encountered with NEEs prepared by track-etched polycarbonate membranes [65], or with NEAs suitably prepared [66]. Note that completely different behaviors can be observed in the case of arrays composed by a small number of nanoelectrodes, where border effects play a relevant role [79].

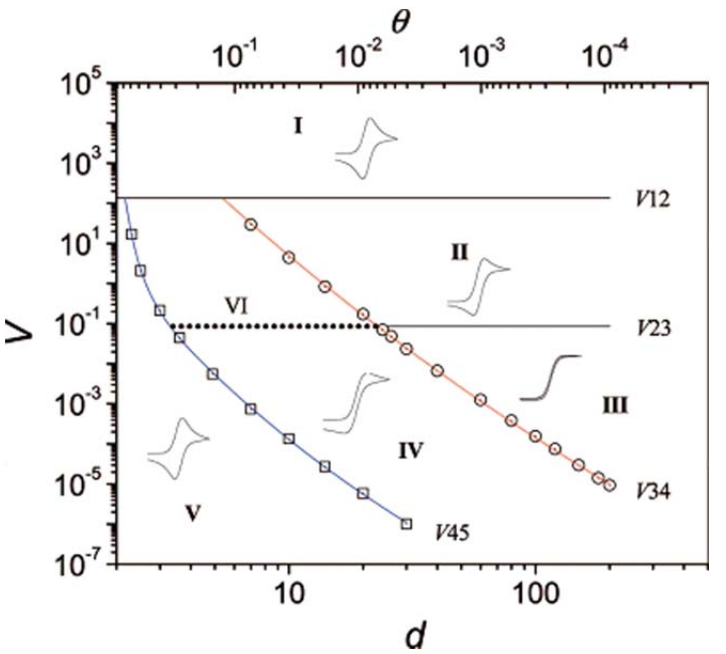

Figure 13. Zone diagram of cyclic voltammetric behavior at microelectrode arrays. d is the center-to center distance of individual electrodes in the array (measured in units of a), V is the dimensionless scan rate, and θ is the fraction of electrochemically active area in the array [75]. Reprinted with permission from Guo, J. et al. *Anal. Chem.* 2009, *81*, 130-138. Copyright © 2009, American Chemical Society.

6.2. Current Signals at NEEs

The diffusion regime usually observed at NEEs, fabricated from commercially available track-etched membrane, is the total overlap regime [2], nevertheless, transition from one regime as a function of the nanoelements distance has been experimentally demonstrated using specially-made membranes [73]. It was recently shown that, for NEE, the transition from the total overlap to the pure radial regime can be observed by increasing the electrolyte viscosity [80]. The voltammetric patterns recorded at NEEs in high viscosity ionic liquids are indeed peak shaped CV at low scan rates, while they become sigmoidally shaped at high scan rate (see Figure 14).

Note that the diffusion coefficient, D, decreases at increasing viscosity, so that diffusion hemispheres around each nanoelectrodes are smaller in a high viscosity medium.

Coming back to the more common situation of the voltammetric use of NEEs in aqueous media, it is worth stressing that, for electroanalytical purposes, the main advantage of the total overlap regime is the enhanced detection limit with regards to conventional electrodes with the same surface area. This is because at NEEs, operating under total overlap diffusion conditions, the Faradaic current (I_F) is proportional to the total geometric area of the ensemble exposed to the sample solution (A_{geom}, area of the nanodisks plus the insulator area), while the double layer capacitive current (I_C), which is the main component of the noise in electroanalytical chemistry, is proportional only to the nanodisks area (active area, A_{act}) [2].

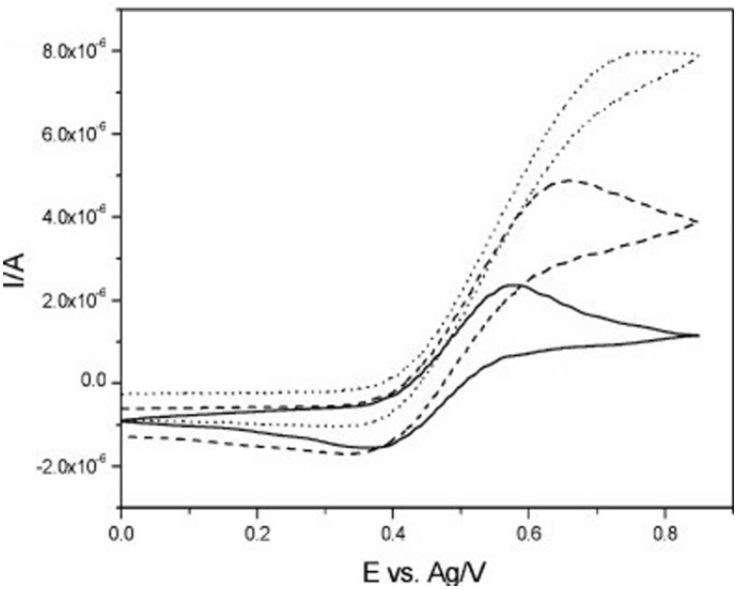

Figure 14. Cyclic voltammograms recorded at different scan rates at a NEE (geometric area 0.07 cm^2; active area 0.004 cm^2), 50 mM Ferrocene (Fc) in [tris(n-hexyl)tetradecylphosphonium] [bis(trifluoromethylsulfonyl)amide]. Scan rates: full line 5 mV/s; dashed line 50 mV s^{-1}; dotted line 500 mV/s [80]. Reprinted with permission from Ugo, P. et al. *Electrochim. Acta* 2010, *55*, 2865-2872. Copyright © 2010, Elsevier.

Typical values for the geometric area range from 0.008 to 0.580 cm^2, [65] this parameter is defined at the moment of the NEE fabrication from the dimension of the hole punched into the insulator. The active area can be easily calculated according to the membrane characteristics such as, pore density (*q*) and mean pore radius (*r*), following the equation reported below:

$$A_{act} = \pi r^2 q A_{geom} \quad (1)$$

The ratio between the active and the geometric area defines a key parameter which takes the name of fractional electrode area (*f*):

$$f = A_{act} / A_{geom} \quad (2)$$

Faradic-to-capacitive currents at NEEs and conventional electrodes with the same geometric area are related by eq. 3 [81]:

$$(I_F/I_C)_{NEE} = (I_F/I_C)_{conv} f \quad (3)$$

Being typical *f* values for NEEs between 10^{-3} and 10^{-2}, I_F/I_C ratios at NEEs can be 2-3 orders of magnitude higher than those at conventional electrodes with the same geometric area. Such an improvement in the Faradaic to capacitive currents ratio explains why detection limits (DLs) at NEEs can be 2-3 order of magnitude lower than with conventional electrodes [2,82,83]. Since the improvement in S/N ratios is strictly related to the fractional area, the

electroanalytical performances of NEEs are not affected by any variation in the geometric area as long as the active area changes accordingly, i.e. the f parameter is kept constant [65].

The main analytical advantage of NEEs over conventional macro (mm-sized) or even ultramicro (μm-sized) electrodes is the dramatic lowering of double layer capacitive currents [2,82]; in case of inability to directly characterize the morphology of the electrodes, the lack of this characteristic should be taken into account as a diagnostic parameter to discriminate well-prepared from defective NEEs.

For example voltammograms affected by a large capacitive current, can indicate poor sealing between the nanowires and the surrounding PC insulator or the heavy scratching of the PC membrane caused by an improper handling of the NEE. On the other hand, a radial diffusive contribution to the overall signal, suggests a larger distance between the nanoelectrodes, probably due to only partial filling of the pores with gold [50,64].

6.3. Electron Transfer Kinetics

An important feature of NEEs is that electron transfer kinetics appear slower than those at conventional electrodes[2]. According to the model proposed by Amatore et al. [84], as well as to more recent theoretical models [75,76,77], NEEs behave as a partially blocked surface electrode (PBE), whose current response is identical to that of a naked electrode of the same overall geometric area, but with a smaller apparent heterogeneous rate constant ($k°_{app}$) for the electron transfer which decreases as the coverage of the surface increases. According to this model, the nanodisks electrodes are the unblocked surface and the template membrane is the blocking material.

The apparent rate constant is related to the true heterogeneous standard rate constant ($k°$) by the following equation:

$$k°_{app} = k°(1 - \vartheta) = k° f \tag{4}$$

where $\vartheta = (A_{geom} - A_{act})/A_{geom}$ and f is the fractional electrode area (see eq. 2).

From an analytical viewpoint, the operativity of eq. 4 means that high Faradic currents can be achieved on redox couples with “very reversible” behavior. In cyclic voltammetry (CV) in fact, the reversibility of a redox system depends on $k°$ value and the scan rate. Using conventional electrodes, reversible patterns are obtained when:

$$v^{1/2} \leq (k° / 0.3) \tag{5}$$

(where v is the scan rate), but if NEEs are used, $k°$ is substituted by $k°_{app}$, and the previous relation becomes:

$$v^{1/2} \leq [(k° f) / 0.3] \tag{6}$$

Considering that mean f values ranges from 10^{-2} to 10^{-3}, from eq. 6 we can conclude that for a certain redox couple, the scan rate value that defines the transition between reversible and quasi-reversible behavior will be placed at 2-3 orders of magnitude lower than those at

conventional electrodes. Note that such a boundary scan rate will decrease with *f* decreasing. This is a limitation to be seriously taken into account when trying to optimize NEEs for analytical application, since it is important to consider the contrasting effect both of the increased I_F/I_C value and the apparent slowing down of the electron transfer kinetics.

On the other hand, from a mechanistic viewpoint, it is an advantage since it means that with NEEs it is easier to measure experimentally very large $k°$ values. Values of $k°_{app}$ are measured typically by CV operating within a scan rate range where the redox system behaves quasi reversibly [85]. By the analysis of ΔE_p dependence on the scan rate [86], and using suitable working curves [87], smaller $k°_{app}$ values are obtained and converted to larger $k°$ by eq. 4 [8,83].

6.4 Current Signals at Nanolithographated NEAs

As explained in paragraph 5, the use of advanced nanolithographic methods allows one to obtain ordered arrays of nanoelectrodes with controlled geometry. The role of the distance/radius of the nanoelectrodes, as well as of their number (with respect to the negligibility of border effects) has been already explained in section 6.1. For NEA, the possibility to control the geometry of the electrodes in the array allows one to obtain, electrode array which operate under pure radial control rather than under total overlap conditions (see Figure 15).

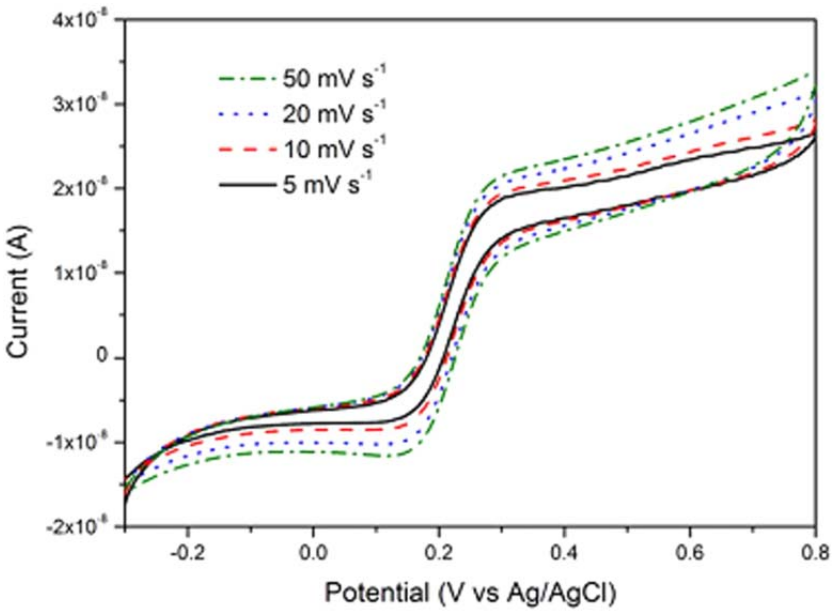

Figure 15. CVs recorded in 10^{-4} M Ferrocene methanol (FE) and 0.5 M $NaNO_3$. Scan rates: 5 (full line), 10 (dash line), 20 (dot line) and 50 mV s^{-1} (dash-dot line). Geometrical characteristics: nanodisk radius = 75 nm, distance centre to centre = 3 μm, estimated number of nanoelectrodes in the array = 1.1 x 10^4 [66]. Reprinted with permission from Moretto, L. M. et al. *Nanotechnology* 2011, *22*, 185305-185312. Copyright © 2011, IOP Publishing.

However, it is worth to stress that, because of the nanolithographic process itself, quite often, the nanoelectrodes obtained are slightly recessed, so that theoretical model for such geometries must be taken into account [66,67].

6.5. Electroanalysis with NEE

Both NEEs and NEAs can be used for interesting analytical applications. However, it can be noted that NEAs with reliable electroanalytical characteristics have been described only very recently, while the "electroanalytical history" of NEEs is longer (starting from1995 [2]) and richer with application examples. For this reason, in the following we will focus on the electroanalytical applications of NEEs.

The improved S/N ratio typical of NEEs facilitates the direct determination of electroactive species at low concentration levels. Besides of application for trace electroanalysis at well known reversible redox probes and analytes [2,82], NEEs has proven to be useful tools for CV analysis of more electrochemically complex systems, such as phenothiazines, methylviologen [83] and the heme-protein cytochrome *c* [88]. In this case, well resolved voltammograms were obtained in diluted solutions of the protein both with and without promoters such as 4-4'-bipiridyl typically used in promoting cytochrome *c* electrochemistry at conventional electrodes [89,90,91]. These promoters are generally required to avoid adsorption/denaturation [92,93] of cytochrome *c* on the Au surface. However, such an adsorption is concentration dependent so that lowering the cytochrome *c* concentration in solution below the adsorption limit (possible at NEEs) can overcome adsorption-related problems [88].

Recently it was shown that DLs achievable with NEEs can be improved by using pulsed voltammetric techniques instead of CV [65]. In particular square wave voltammetry (SWV) at low frequency was suitable for determining trace of iodide in real samples such as lagoon waters. It was observed that both the peak height and the resolution (given by the ratio $I_p/W_{1/2}$, where I_p is the peak current and $W_{1/2}$ is the half-peak width) reach their maximum at low frequencies. This is explained by the geometry of the NEEs and the time dependence of the diffusion layers. At low time scale, that is at low frequencies, diffusion hemispheres around each nanodisk are larger, so that the total overlap condition is achieved. Note that, as explained in paragraph 6.2, in total overlap regime all the geometric area (A_{geom}) contributes to the Faradic current, so that the voltammetric signal is higher than in partial overlap conditions. Besides, not reaching the DL obtained using mercury drop electrode, NEEs proved to be preferable when direct detection is required and when preconcentration and deoxygenation is not possible [94]. This reason together with the easy miniaturization, make NEEs good candidates for their application for *in-situ* environmental analyses and in automated integrated electroanalytical systems [95].

NEEs have been applied for the determination of other important environmental analytes such as arsenic [96]. The electrochemical technique of choice was anodic stripping-square wave voltammetry (AS-SWV). In this technique, the analyte of interest is deposited (reduced) on the working electrode during a Faradic preconcentration step, and subsequently oxidized from the electrode during the stripping step. The current measured during the stripping step is used to determine the analyte concentration. Albeit NEEs furnished DLs two orders of magnitude lower than conventional gold macro electrodes, they presented a shorter linearity

range. This is due to the fact that, in the preconcentration step, arsenic is reduced on the active surface of the NEE (i.e. on the gold nanodisks), and, for high arsenic concentration, the gold disks are easily saturated. For such characteristics the use of NEEs is advisable and advantageous mainly for anodic stripping voltammetry (ASV) analyses at trace and ultratrace concentration levels. Figure 16 shows the square wave voltammograms for the electrochemical determination of As (III) using a gold NEE.

The small active area od NEEs can be a limit also when the gold nanodisks are used as substrate for the immobilization of bioactive molecules, as typically done for preparing electrochemicalbiosensors. A possible way to increasethe active surface area at NEEs, is performing the partial etching of the polycarbonate of the templating membrane. This procedure causes the structure of the final ensemble to change from a flat 2D surface made of metal nanodisks imbedded in a non conductive substrate to a 3D structure made by an ensemble of nanowires partially protruding from the insulating layer. 3D-NEEs were obtained from 2D-NEEs by two different methods. The first one, proposed by Martin et al. [61], exploits a O_2/Ar plasma to etch in a controlled way the templating polymer. A simpler method, proposed by Zoski et al. [60], is based on substituting the plasma-etching with a chemical etching by using suitable solvents to partially dissolve the polycarbonate. A suitable mixture ratio, for a controlled etching rate, was found 50:50 CH_2Cl_2/C_2H_5OH.

When an etching treatment is performed, the measurement of the active area is often desirable in order to correlate the intensity of electrochemical signals with A_{act} values . For the evaluation of the increase of the active surface area, different electrochemical approaches have been proposed, such as: AC electrochemical impedance spectroscopy [97], measurement of the amount of charge of gold oxide stripping [98] and the measurement of total charge associated to the redox reaction of an adsorbed specie such as polyoxometalates [59].

Techniques which relies on diffusion controlled soluble species, i.e. impedance spectroscopy, does not take into account the microscopic roughness of the nanowires. However, for electrochemical applications where electrochemical reactions depend on surface properties such as adsorption, the roughness of the structures cannot be neglected and require an area determination technique involving a surface active specie, i.e. polyoxometalates [59].

Cao et al. [97,98] exploited the enhanced active surface area of 3D-NEEs for the detection of the chemotherapeutic agent Danurobicin. In this approach the analyte is adsorbed on the gold nanowires surface and directly analyzed by SWV [98]. The functionalization of the nanowires with L-cysteine increased the amount of adsorbed analyte, giving lower detection limits [97].

3D-NEEs have been applied also as sensitive biosensor for DNA-hybridization detection [99,100]. Single stranded DNA can be immobilized both on the gold nanorods surface of 3D-NEEs [99,100] or on the polymer membrane surface [101]. In the former case the detection mechanism exploits an electrocatalytic reaction between a primary acceptor, namely $Ru(NH_3)_6^{3+}$ and a secondary acceptor, namely $Fe(CN)_6^{3-}$. The first ion is reduced at the electrode surface and then reoxidized by the anion, producing an electrocatalytic process. By increasing the concentration of negatively charged phosphate groups at the Au surface of NEEs, by hybridization with complementary sequences, the local concentration of $Ru(NH_3)_6^{3+}$ increases as well (Figure 17).

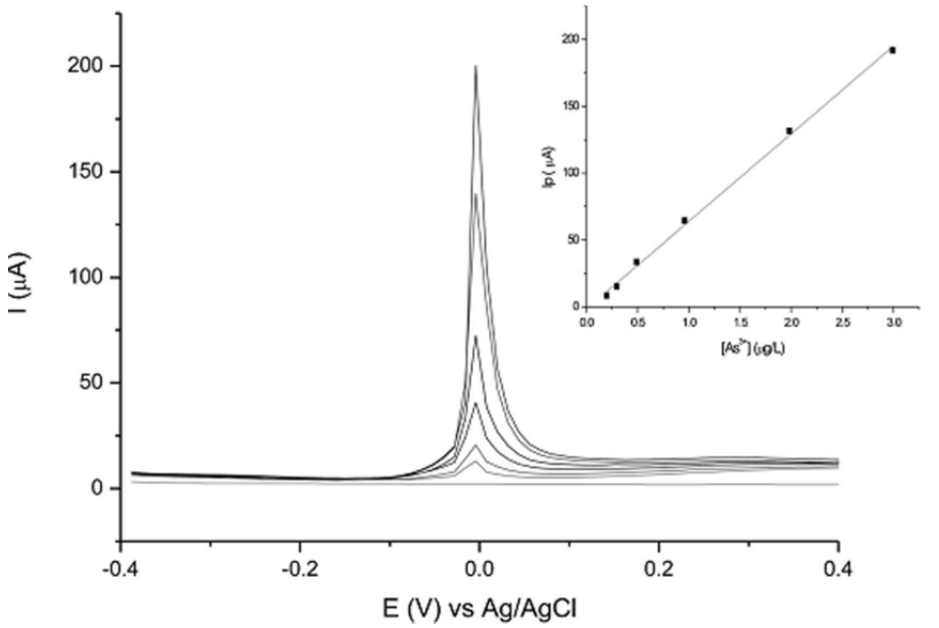

Figure 16. AS-SWV at NEE at different As (III) concentrations (0 - 0.3 μg/L). Inset: calibration plot [96]. Reprinted with permission from Mardegan, A. et al. *Electroanal.* 2012, *24*, 798-806. Copyright © 2012, Wiley-VCH.

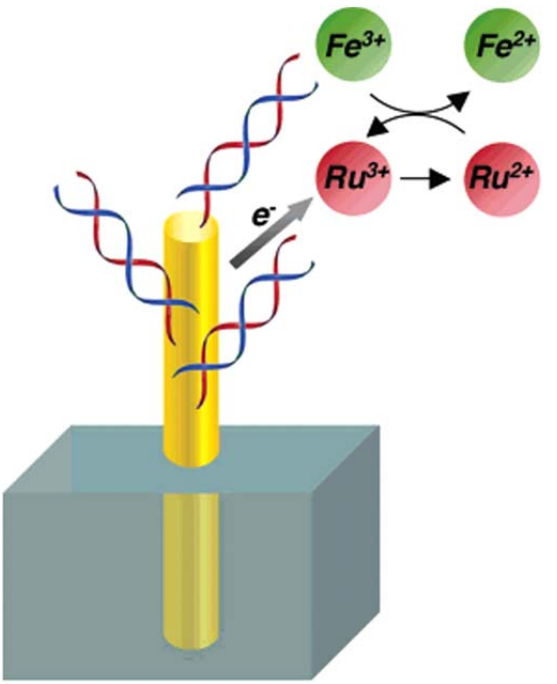

Figure 17. Schematic illustration of Ru(III)/Fe(III) electrocatalysis at a DNA-modified Au NEE [100]. Reprinted with permission from Lapierre-Devlin, M. A. et al. *Nano Lett.* 2005, *5*, 1051-1055. Copyright © 2005, American Chemical Society.

Functionalization of the gold surface on a 3D-NEE has also been applied in the determination of the ovarian cancer marker Mucin-16 (MUC-16) [102]. Viswanathan et al. developed an electrochemical immunosensor using ferrocene carboxylic acid encapsulated liposomes bonded with monoclonal anti-Mucin-16 antibodies (αMUC-16). α MUC-16 was immobilized on a self-assembled monolayer of cysteamine on the 3D-NEE via cross-linking with carbodiimide (EDC) and N-hydroxysulfosuccinimide (Sulfo-NHS). A sandwich immunoassay was performed on α MUC-16 functionalized 3D-NEE with MUC-16 and immunoliposomes. Differential pulse voltammetry was employed to quantify the faradic redox response of ferrocene carboxylic acid released from immunoliposomes and quantify the MUC-16 concentration (Figure 18). The results obtained with this immunosensor were in good correlation with commercial ELISA test performed on the same samples, proving functionalized 3D-NEEs being a viable alternative especially for the development of home testing kits.

The exploitation of etched 3D-NEEs in order to increase the amount of adsorbed biomolecules on the gold nanowires surface, proved to be a viable process, the drawback is an increase of the capacitive current and, consequently, an increase of the S/N ratio [59]. A different approach has been recently proposed where the biorecognition element is immobilized on the polymeric matrix of the NEE [70,71]. In such a design, transducer and biorecognition elements are not overlapped but integrated in strict proximity. This approach, besides maintaining the excellent detection limits of 2D-NEEs, greatly increases the amount of biomolecules bound on the NEE, since the PC surface is 2-3 orders of magnitude larger than the gold surface of the nanoelectrodes, i.e. A_{act} Pozzi Mucelli et al. [71] proposed this strategy for the preparation of an immunosensor for the determination of the HER2 receptor, overexpressed in certain kinds of breast cancer. At first, the specific antibody trastuzumab is immobilized on the PC of a NEE. Later on, it is incubated with the sample to capture the target protein HER2. The captured protein is then reacted with a different primary antibody (namely, monoclonal CB-11) which finally binds a secondary antibodylabeled with horseradish peroxidase (HRP. The electrochemical signal is generated by methylene blue (MB) added to the solution as redox mediator, which shuttles electrons from the nanoelectrode elements to the HRP, when the latter reacts with its substrate, i.e. H_2O_2, (added in the solution ; see Figure 19). The same principles were also applied for the electrochemical detection of single chain fragment variable proteins [70].

In some cases, aspecific adsorption of the proteins on the gold nanodisks surface has been observed, limiting the electrochemical signal and consequently the detection efficiency in NEE-based biosensors. In order to overcome this problem, it is possible to protect the nanoelectrodes with a self-assembled monolayer (SAM) of short chains thiols. This functionalization prevents protein fouling of the NEEs allowing the detection of well resolved voltammograms of the probe molecule [103]. In order to characterize the obtained structures a careful AFM characterization of the NEEs was performed.

Recently, the immobilization of biorecognition probes onto the PC of NEEs was used for the detection of DNA-hybridization [101]. Single-stranded amino-terminated DNA probes (ssDNA) were bound onto the PC by exploiting the reactivity of the carboxylic groups present on the polycarbonate surface.

\

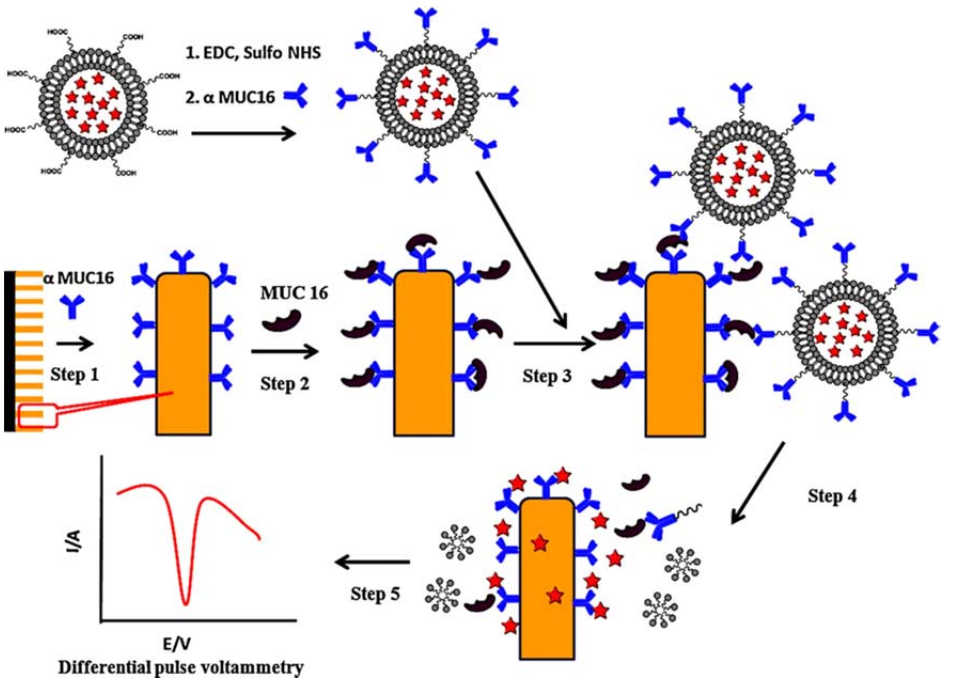

Figure 18. Sketch of the electrochemical MUC-16 detection method. Step 1 αMUC16 immobilized on the 3D-NEE exposed wires. Step 2 MUC-16 immunoconiugated with the antibody on the nanowires surface. Step 3 sandwich immunocomplex with immunoliposomes. Step 4 disruption of immunoliposomes and release of the redox specie, whose concentration is determined by SWV (step 5) [102]. Reprinted with permission from Viswanathan, S. *Anal. Chim. Acta* 2012, *726*, 79-84. Copyright © 2012, Elsevier.

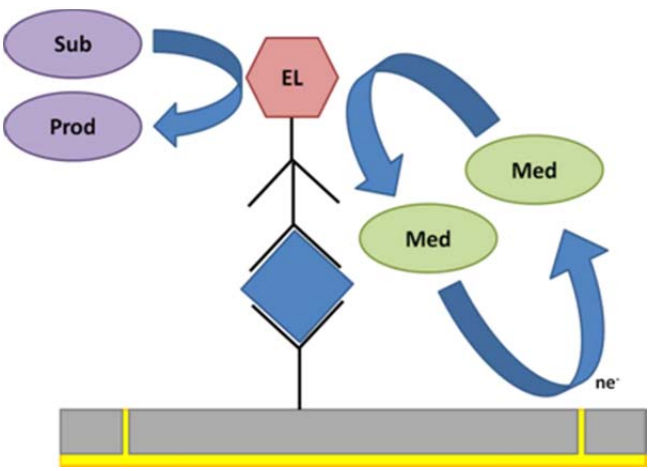

Figure 19. Schematic illustration of the HER2 detection mechanism. A specific antibody (trastuzumab) is first attached to the polycarbonate to capture the target protein HER2 (blue square). Another primary antibody (CB-11) binds to the target protein and subsequently with a secondary antibody labeledd with an enzyme (EL);the reaction of EL with the substrate (Sub) and the mediator (Med), generates the electrochemical signal.

Titrations with thionin acetate indicate that a surface concentration of -COOH in the order of 9.7×10^{-10} mol cm^{-2} is naturally present on the surface of track-etched PC; this number can be increased to 3.4×10^{-9} mol cm^{-2}, by controlled oxidation with $KMnO_4$. The reactions used for the immobilization [101] are summarized in the following scheme:

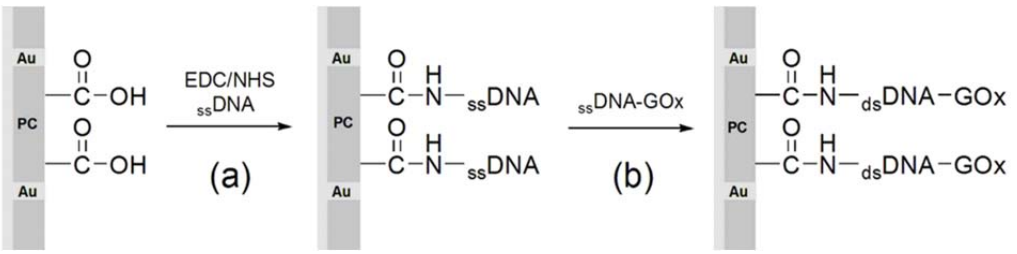

Figure 20. Design of DNA hybridization sensor based on NEE assembly: (a) activation of -COOH groups of the PC surface and immobilization of the capture amino-end DNA probe onto the activated carboxylic functionalities and (b) hybridization of DNA-GOx conjugate onto modified PC surface.

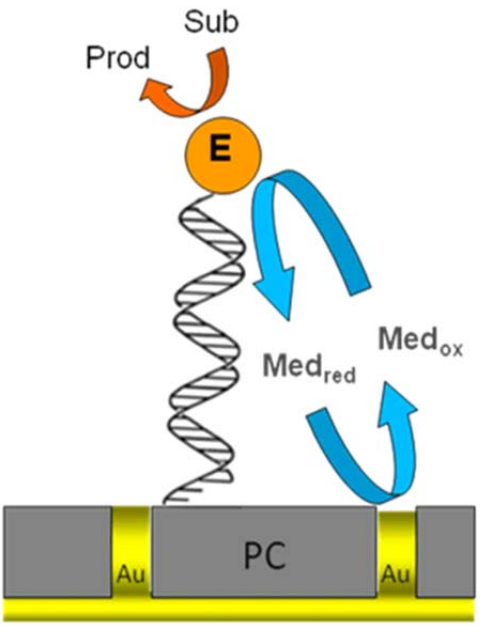

Figure 21. Schematic illustration of two DNA biorecognition systems The probe DNA strand is first attached to the polymer membrane, the target GOx-conjugated strand is then hybridized. The mediator reacts with the reduced enzyme and gives an electrochemical signal at the nanoelectrodes.

NEEs functionalized with the DNA probe are then hybridized with the target ssDNA labeled with glucose oxidase (GOx) [104]. The occurrence of the hybridization event is detected by adding, to the supporting electrolyte, excess glucose as the substrate and the (ferrocenylmethyl) trimethylammonium cation (FA^+) as suitable redox mediator. In the case of positive hybridization, an electrocatalytic current is detected. In the proposed sensor, the biorecognition event and signal transduction occur in different ways at neighboring sites, i.e. the PC surface and the nanoelectrodes, respectively. These sites are separated albeit in close

proximity on a nanometer scale (see Figure 21). The proposed biosensor displays high selectivity and sensitivity, with the capability to detect few hundreds femtomoles of target DNA.

CONCLUSION

Nanoelectrodes ensemble and arrays can be obtained by template deposition in self-standing track-etched polymer membranes or on thin polymer films in which ordered arrays of holes are obtained by advanced nanolithographic techniques. The final result is indeed a composite material in which nanowires or nanorods of a metal conductor are inserted into a polymer matrix. The control of the geometry of the composite allows one to obtain functional materials with unique electroanalytical characteristics.

NEEs and NEAs demonstrate a dramatic enhancement of the signal to background current ratio with respect to other electrode systems, however the drawbacks being the operativity of such performances mainly with reversible redox systems. Moreover the small active area can limit their modifications by adsorption of active molecules. Such limits can be overcome when NEEs are used in electrochemical biosensors where electron transfer processes are tuned by the electrochemistry of suitable reversible mediators. Moreover, the active area can be suitably increased by the controlled etching of the polymeric membrane. Future research efforts should be devoted to the development of singly addressable electrodes. The possibility to move from present NEEs (where all nanoelectrodes are interconnected each other) to more sophisticated nanoelectrodes systems (where multiple analyte determination is achieved) as well as the extreme miniaturization of such devices, would be particularly suitable for sensors to be used in the bioanalytical field, both for “in vitro” and “in vivo” analyses. However, the advantages coming from the availability of multianalytes sensors are obvious also for environmental or food analyses and for materials testing as well.

Finally, it is worth stressing that further advantages can be pointed out due to the composite nature of NEEs/NEAs. They are indeed composed of metal nanoelements surrounded by a (relatively) wide surface of a suitable polymer. Recent studies showed that a wide polymer surface can be exploited for functionalization process, by immobilizing on it molecule layers with biorecognition capabilities, which can be coupled, by a suitable redox cycle, with the electrochemical transduction capabilities of the metal nanoelectrodes.

ACKNOWLEDGMENT

Financial support by MIUR(Rome), project 2010AXENJ8, is acknowledged.

REFERENCES

[1] Martin, C. R. (1999). In *Electroanalytical Chemistry;* Editors, A. J. Bard; I. Rubinstein, Marcel Dekker: New York, Vol. *21*, 1-74.

[2] Menon, V. P. & Martin, C. R. (1995). *Anal. Chem.*, *67*, 1920-1928.
[3] Possin, G. E. (1970). *Rev. Sci. Instrum.*, *41*, 772-774.
[4] Williams, W. D. & Giordano, N. (1984). *Rev. Sci. Instrum.*, *55*, 410-412.
[5] Routkevitch, D., Bigioni, T., Moskovits, M. & Xu, J.-M. (1996). *J. Phys. Chem.*, *100*, 14037-14047.
[6] Schoennberger, C., van der Zande, B. M. I., Fokkink, L. G. J., Henny, M., Schmid, C., Kruger, M., Bachtold, A., Huber, R., Birk, H. & Staufer, U. (1997). *J. Phys. Chem. B*, *101*, 5497-5505.
[7] Zheng, M., Li, G., Zhang, X., Huang, S., Lei, Y. & Zhang, L. (2001). *Chem. Mater.*, *13*, 3859-3861.
[8] Sabatani, E. & Rubinstein, J. (1987). *J. Phys. Chem.*, *91*, 6663-6669.
[9] Chailapakul, O., Sun, L., Xu, C. J. & Crooks, R. M. (1993). *J. Am. Chem.Soc.*, *115*, 12459-12467.
[10] Che, G. L. & Cabrera, C. R. (1996). *J. Electroanal. Chem.*, *417*, 155-161.
[11] Jeonng, E., Galow, T. H., Schotter, J., Bal, M., Ursache, A., Tuominen, M. T., Stafford, C. M., Russel, T. P. & Rotello, V. M. (2001). *Langmuir*, *17*, 6396-6398.
[12] Cheng, W., Dong, S. & Wang, E. (2002). *Anal. Chem.*, *74*, 3599-3604.
[13] Pantano, P. & Walt, D. R. (1997). *Rev. Sci. Instrum.*, *68*, 1357-1359.
[14] Tam, J. M., Szunerits, S. & Walt, D. R. (2003). In *Encyclopedia of Nanoscience and Technology;* Editor, H. S. Naiwa, American Scientific Publishers: Stevenson Ranch, Vol. *8*, 167-177.
[15] Chovin, A., Garrigue, P., Vinatier, P. & Sojic, N. (2004). *Anal. Chem.*, *76*, 357-364.
[16] Zamuner, M., Talaga, D., Deiss, F., Guieu, V., Kuhn, A., Ugo, P. & Sojic, N. (2009). *Adv. Funct. Mater.*, *19*, 3129-3135.
[17] Penner, R. M. & Martin, C. R. (1987). *Anal. Chem.*, 59, 2625-2630.
[18] De Leo, M., Pereira, F. C., Moretto, L. M., Scopece, P., Polizzi, S. & Ugo, P. (2007). *Chem. Mat.*, *19*, 5955-5964.
[19] Gilliam, R. J., Thorpe, S. J. & Kirk, D. J. W. (2006). *Appl. Electrochem.*, *37*, 233-239.
[20] Harrell, C. C., Lee, S. B. & Martin, C. R. (2003). *Anal. Chem.*, *75*, 6861-6867.
[21] Apel, P. Y. (2001). *Radiat. Meas.*, *34*, 559-566.
[22] Apel, P. Y., Korchev, Y. E., Siwy, Z., Spohr, R. & Yoshida, M. (2001). *Nucl. Instrum. Methods Phys. Res. B*, *184*, 337-346.
[23] Fleisher, R. L., Price, P. B. & Walker, R. M. (1975). *Nuclear Tracks in Solids: Principle and Applications*, University of California Press: Berkley.
[24] Siwy, Z., Apel, P. Y., Baur, D., Dobrev, D. D., Korchev, Y. E., Neumann, R., Spohr, R., Trautmann, C. & Voss, K.-O. (2003). *Surf. Sci*, *532*, 1061-1066.
[25] Trautman, C., Bruchle, W., Spohr, R., Vetter, J. & Angert, N. (1996). *Nucl. Instrum. Methods Phys. Res. Sect. B*, *111*, 70-74.
[26] Klintberg, L., Lindberg, M. & Thornell, G. (2001). *Nucl. Instrum. Methods Phys. Res. Sect. B*, *184*, 536-543.
[27] Ferain, R. (2001). Legras *Nucl. Instrum. Methods B*, *174*, 116–122.
[28] Li, N., Yu, S., Harrell, C. C. & Martin, C. R. (2004). *Anal. Chem.*, *76*, 2025-2030.
[29] Bean, C. P. & De Sorbo, W. (1968). US Patent 3,770,532-19731 106 (9 February).
[30] Siwy, Z., Dobrev, D., Neumann, R., Trautmann, C. & Voss, K. (2003). *Appl. Phys. A*, *76*, 781-785.

[31] Scopece, P., Baker, L. A., Ugo, P. & Martin, C. R. (2006). *Nanotechnology*, *17*, 3951-3956.
[32] Oleinikof, V. A., Tolmachyova, Y. V., Berezkin, V. V., Vilensky, A. I. & Mchedlishvili, B. V. (1995). *Radiat. Meas.*, *25*, 713-714.
[33] Kececi, K., Sexton, L. T., Buyukserin, F. & Martin, C. R. (2008). *Nanomedicine UK*, *3*, 787-796.
[34] Wang, J. & Martin, C. R. (2008). *Nanomedicine UK*, *3*, 13-20.
[35] Heins, E. A., Siwy, Z. S., Baker, L. A. & Martin, C. R. (2005). *Nano Lett.*, *5*, 1824-1829.
[36] Gambirasi, A., Cattarin, S., Musiani, M., Vázquez-Gómez, L. & Verlato, E. (2011). *Electrochim. Acta*, *56*, 8582-8588.
[37] Konishi, Y., Motoyama, M., Matsushima, H., Fukunaka, Y., Ishii, R. & Ito, Y. (2003). *J. Electroanal. Chem.*, *559*, 149-153.
[38] Motoyama, M., Fukunaka, Y., Sakka, T., Ogata, Y. H. & Kikuchi, S. (2005). *J. Electroanal. Chem.*, *584*, 84-91.
[39] Piraux, L., Duboix S. & Champagne, S. (1997). *Nucl. Inst. Meth. Phys. Res. B*, *131*, 357-363.
[40] Chiriac, H., Moga, A. E., Urse, M. & Ovari, T.-A. (2003). *Sens. Actuators A*, *106*, 348-351.
[41] Pirota, K. R., Navas, D., Hernandez-Vélez, M., Nielsch, K. & Vasquez, M. (2004). *J. Alloy Compd.* 2004, *369*, 18-26.
[42] Platt, M., Dryfeand, R. A. W. & Robaerts, E. P. L. (2004). *Electrochim. Acta*, *49*, 3937-3945.
[43] Prieto, A. L., Sander, M. S., Gonzalez, M. S. M., Gronsky, R., Sands, T. & Stacy, A. M. (2001). *J. Am. Chem. Soc.*, *123*, 7160-7161.
[44] Ruktevich, D., Bigioni, T., Moskovits, M. & Xu, J. M. (1996). *J. Phys. Chem.*, *100*, 14037-14047.
[45] Tian, M. L., Wang, J., Kurtz, J., Mallouk, T. E. & Chan, M. H. W. (2003). *Nano Lett.*, *3*, 919-923.
[46] Tian, M. L., Wang, J., Snyder, J., Kurtz, J., Liu, Y., Schiffer, P., Mallouk, T. E. & Chan, M. H. W. (2003). *Appl Phys. Lett*., *83*, 1620-1622.
[47] Wang, J., Tian, M. L., Mallouk, T. E. & Chan, M. H. W. (2004). *J. Phys. Chem. B*, *108*, 841-845.
[48] Wang, J. G., Tian, M. L., Mallouk, T. E. & Chan, M. H. W. (2004). *Nano Lett*., *4*, 1313-1318.
[49] Paunovic, M. & Schlesinger, M. (2000). *Modern Electroplating*, Wiley: New York.
[50] Pereira, F.C., Moretto, L.M., De Leo, M., Boldrin Zanoni, M.V. & Ugo, P., (2006), *Anal. Chim. Acta,* 575, 16-24.
[51] De Leo, M., Pereira, F.C., Moretto, L.M., Scopece, P., Polizzi, S. & Ugo, P. (2007). *Chem. Mater*.,19, 5955-5964
[52] Jirage, K. B., Hulteen, J. C. & Martin, C. R. (1997). *Science*, *278*, 655-658.
[53] Hulteen, J. C., Jirage, K. B. & Martin, C. R. (1998). *J. Am. Chem. Soc.*, *120*, 6603-6604.
[54] Jirage, K. B., Hulteen, J. C. & Martin, C. R. (1999). *Anal. Chem.*, *71*, 4913-4918.
[55] Kobayashi, Y. & Martin, C. R. (1999). *Anal. Chem.*, *71*, 3665-3672.
[56] Bercu, B., Enculescu, I. & Spohr, R. (2004). *Nucl.Instrum. Meth. B*, *225*, 497-502.

[57] Dryfe, R. A. W., Simm, A. O. & Kralj B. (2003). *J. Am. Chem. Soc*., *125*, 13014-13015.
[58] Tai, Y.-L. & Teng, H. (2004). *Chem. Mater.*, *16*, 338-342.
[59] De Leo, M., Kuhn, A. & Ugo, P. (2007). *Electroanalysis*, *19*, 227-236.
[60] Krishnamoorthy, K. & Zoski, C. G. (2005). *Anal. Chem.*, *77*, 5068-5071.
[61] Yu, S., Li, N., Wharton, J. & Martin, C. R. (2003). *Nano Lett.*, *3*, 815-818.
[62] Ugo, P., Moretto, L. M. & Vezzà, F. (2002). *ChemPhysChem.*, *3*, 917-925.
[63] Ugo, P. (2005). In *Encyclopedia of sensors*; Editors, C. A. Grimes, E. C. Dickey, M. V. Pishko, American Scientific Publishers: Stevenson Ranch, Vol. *8*, 67-86.
[64] Ugo, P. & Moretto, L. M. (2007). In *Handbook of Electrochemistry*; Editor, C. Zoski, Elsevier: Amsterdam, 678-709.
[65] Moretto, L. M., Pepe, N. & Ugo P. (2004). *Talanta*, *62*, 1055-1060.
[66] Moretto, L. M., Tormen, M., De Leo, M., Carpentiero, A. & Ugo, P. (2011). *Nanotechnology*, *22*, 185305-185312.
[67] Lanyon, Y. H., De Marzi, G., Watson, Y. E., Quinn, A. J., Gleeson, J. P., Redmond, G. & Arrigan, D. W. M. (2007). *Anal. Chem.*, *79*, 3048-3055.
[68] Errachid, A., Mills, C. A., Pla-Roca, M., Lopez, M. J., Villanueva, G., Bausells, J., Crespo, E., Teixidor, F. & Samitier, J. (2008). *Mater. Sci. Eng. C*, *28*, 777-780.
[69] Madison, M. Z. & Cooper, J. M. (2006). *Lab. Chip*, *6*, 1020-1025.
[70] Zamuner, M., Pozzi Mucelli, S., Tormen, M., Stanta, G. & Ugo, P. (2008). *Eur. J. Nanomed.*, *1*, 33-36.
[71] Pozzi Mucelli, S., Zamuner, M., Tormen, M., Stanta, G. & Ugo, P. (2008). *Biosens. Bioelectron.*, *23*, 1900-1903.
[72] Lee, H. J., Beriet, C., Ferrigno, R. & Girault, H. H. (2001). *J. Electroanal. Chem.*, *502*, 138-145.
[73] Hulteen, J. C., Menon, V. P. & Martin, C. R. (1996). *J. Chem. Soc. Faraday T.*, *92*, 4029-4032.
[74] Cheng, J. F., Whitley, L. D. & Martin, C. R. (1989). *Anal. Chem.*, *61*, 762-766.
[75] Guo, J. & Lindner, E. (2009). *Anal. Chem.*, *81*, 130-138.
[76] Davies, T. J. & Compton, R. G. (2005). *J. Electroanal. Chem.*, *585*, 63-82.
[77] Huang, X-J., O'Mahony, A. M. & Compton, R. G. (2009). *Small*, *7*, 776-788.
[78] Amatore, C., Oleinik, A. I. & Svir, I. (2009). *Anal. Chem.*, *81*, 4397-4405.
[79] Godino, N., Borrise, X., Munoz, F. X., del Campo, F. J. & Compton, R. G. (2009). *J. Phys. Chem. C*, *113*, 11119-11125.
[80] Ugo, P., Moretto, L. M., De Leo, M., Doherty, A. P., Vallese, C. & Pentlavalli, S. (2010). *Electrochim. Acta*, *55*, 2865-2872.
[81] Ugo, P., Moretto, L. M. & Vezzà, F. (2003). In *Sensors Update*; Editors, H. Baltes, G. K. Fedder, J. G. Korvink, Wiley-VCH: Weinheim, Vol. *12*, 121-140.
[82] Ugo, P., Moretto, L. M., Bellomi, S., Menon, V. P. & Martin, C. R. (1996). *Anal. Chem.*, *68*, 4160-4165.
[83] Brunetti, B., Ugo, P., Moretto, L. M. & Martin, C. R. (2000). *J. Electroanal. Chem.*, *491*, 166-174.
[84] Amatore, C., Saveant, J. M. & Tessier, D. (1983). *J. Electroanal. Chem.*, *147*, 39-51.
[85] Bard, A. J. & Faulkner, L. (2000). *Electrochemical Methods, 2nd ed.,* VCH: Weinheim.
[86] Greef, R., Pea, R., Peter, L. M., Pletcher, D. & Robinson, J. (1985). *Instrumental Methods in Electrochemistry*; Ellis Horwood Ltd.: Chester.
[87] Nicholson, R. S. (1965). *Anal. Chem.*, *37*, 1351-1355.

[88] Ugo, P., Pepe, N., Moretto, L.M. & Battagliarin, M., (2003). *J. Electroanal. Chem., .560,* 51-58.
[89] Eddowes, M. J. & Hill, H. A. O. (1977). *J. Chem. Soc. Chem. Comm.*, 771-772.
[90] Allen P. M., Hill, H. A. O. & Walton, N. J. (1984). *J. Electroanal. Chem.*, *178*, 69-86.
[91] Eddowes, J. M. & Hill, H. A. O. (1979). *J. Am. Chem. Soc.*, *101*, 4461-4462.
[92] Sagara, T., Murakami, H., Igarashi, S., Sato, H. & Niki, K. (1991). *Langmuir*, *7*, 3190-3196.
[93] Sagara, T., Niwa, K., Sone, A., Innen, C. & Niki, K. (1990). *Langmuir*, *6*, 254-262.
[94] Ugo, P., Moretto, L. M., Silvestrini, M. & Pereira, F. C. (2010). *Intern. J. Environ. Anal. Chem.*, *90*, 747-759.
[95] Liao, K.-T., Chen, C.-M., Huang, H.-J. & Lin, C.-H. (2007). *J. Chromatogr. A*, *1165*, 213-218.
[96] Mardegan, A., Scopece, P., Lamberti, F., Meneghetti, M., Moretto, L. M. & Ugo, P. (2012). *Electroanalysis*, *24*, 798-806.
[97] Cao, L., Yan, P., Sun, K. & Kirk D. W. (2008). *Electrochim. Acta*, *53*, 8144-8148.
[98] Cao, L., Yan, P., Sun, K. & Kirk D. W. (2009). *Electroanalysis*, *21*, 1183-1188.
[99] Gasparac, R., Taft, B. J., Lapierre-Devlin, M. A., Lazareck, A. D., Xu, J. M. & Kelley, S. O. (2004). *J. Am. Chem. Soc.*, *126*, 12270-12271.
[100] Lapierre-Devlin, M. A., Asher, C. L., Taft, B. J., Gasparac, R., Roberts, M. A. & Kelley, S. O. (2005). *Nano Lett.*, *5*, 1051-1055.
[101] Silvestrini, M., Fruk, L. & Ugo, P. *Biosens. Bioelectron.* submitted.
[102] Viswanathan, S., Rani, C. & Delerue-Matos, C. (2012). *Anal. Chim. Acta*, *726*, 79-84.
[103] Silvestrini, M., Schiavuta, P., Scopece, P., Pecchielan, G., Moretto, L. M. & Ugo, P. (2011). *Electrochim. Acta*, *56*, 7718-7724.
[104] Fruk, L., Müller, J., Weber, G., Narvaez, A., Dominguez, E. & Niemeyer, C. M. (2007). *Chem. Eur. J.*, *13*, 5223-5231.